In Situ database Analyses Report

Surface drifters

prepared by the Pi-MEP Consortium

June 15, 2023

Contents

Acronym

Aquarius	NASA/CONAE Salinity mission
ASCAT	Advanced Scatterometer
ATBD	Algorithm Theoretical Baseline Document
BLT	Barrier Layer Thickness
CMORPH	CPC MORPHing technique (precipitation analyses)
CPC	Climate Prediction Center
CTD	Instrument used to measure the conductivity, temperature, and pressure of seawater
DM	Delayed Mode
EO	Earth Observation
ESA	European Space Agency
FTP	File Transfer Protocol
GOSUD	Global Ocean Surface Underway Data
GTMBA	The Global Tropical Moored Buoy Array
Ifremer	Institut français de recherche pour l'exploitation de la mer
IPEV	Institut polaire français Paul-Émile Victor
IQR	Interquartile range
ISAS	*In Situ* Analysis System
Kurt	Kurtosis (fourth central moment divided by fourth power of the standard deviation)
L2	Level 2
LEGOS	Laboratoire d'Etudes en Géophysique et Océanographie Spatiales
LOCEAN	Laboratoire d'Océanographie et du Climat : Expérimentations et Approches Numériques
LOPS	Laboratoire d'Océanographie Physique et Spatiale
MDB	Match-up Data Base
MEOP	Marine Mammals Exploring the Oceans Pole to Pole
MLD	Mixed Layer Depth
NCEI	National Centers for Environmental Information
NRT	Near Real Time
NTAS	Northwest Tropical Atlantic Station
OI	Optimal interpolation
Pi-MEP	Pilot-Mission Exploitation Platform
PIRATA	Prediction and Researched Moored Array in the Atlantic
QC	Quality control
R_{sat}	Spatial resolution of the satellite SSS product
RAMA	Research Moored Array for African-Asian-Australian Monsoon Analysis and Prediction
r^2	Square of the Pearson correlation coefficient
RMS	Root mean square
RR	Rain rate
SAMOS	Shipboard Automated Meteorological and Oceanographic System
Skew	Skewness (third central moment divided by the cube of the standard deviation)
SMAP	Soil Moisture Active Passive (NASA mission)
SMOS	Soil Moisture and Ocean Salinity (ESA mission)
SPURS	Salinity Processes in the Upper Ocean Regional Study
SSS	Sea Surface Salinity
SSS_{insitu}	*In situ* SSS data considered for the match-up

SSS_{SAT}	Satellite SSS product considered for the match-up
ΔSSS	Difference between satellite and *in situ* SSS at colocalized point ($\Delta SSS = SSS_{SAT}$- SSS_{insitu})
SST	Sea Surface Temperature
Std	Standard deviation
Std*	Robust Standard deviation = median(abs(x-median (x)))/0.67 (less affected by outliers than Std)
Stratus	Surface buoy located in the eastern tropical Pacific
Survostral	SURVeillance de l'Océan AuSTRAL (Monitoring the Southern Ocean)
TAO	Tropical Atmosphere Ocean
TSG	ThermoSalinoGraph
WHOI	Woods Hole Oceanographic Institution
WHOTS	WHOI Hawaii Ocean Time-series Station
WOA	World Ocean Atlas

1 Overview

This report presents some characteristics of the Surface drifters in situ dataset used by the Pi-MEP to validate SMOS, SMAP and Aquarius satellite SSS products. A series of plots is proposed showing:

- Number of SSS data as a function of time and distance to coast

- Histogram of shallowest salinity and pressure (if relevant)

- Temporal mean of shallowest salinity pressure measurements (if relevant)

- Spatial density of shallowest salinity

- Spatial Maps of the Time-mean and temporal Std of *in situ* and satellite SSS and of the ΔSSS

- Time series of the monthly median and Std of *in situ* and satellite SSS and of the ΔSSS

- Zonal mean and Std of *in situ* and satellite SSS and of the ΔSSS

- Scatterplots of ISAS vs *in situ* SSS by latitudinal bands

- Time series of the monthly median and Std of the ΔSSS sorted by latitudinal bands

- ΔSSS sorted as function of geophysical parameters

- ΔSSS maps and statistics for different geophysical conditions

1.1 In situ dataset

1.1.1 Surface drifters

The skin depth of the L-band radiometer signal over the ocean is about 1 cm whereas classical surface salinity measured by ships or Argo floats are performed at a few meters depth. In order to improve the knowledge of the SSS variability in the first 50 cm depth, to better document the SSS variability in a satellite pixel and to provide ground-truth as close as possible to the sea surface for validating satellite SSS, the L-band remotely sensed community proposed to deploy numerous surface drifters over various parts of the ocean. Surface drifter data are provided by the LOCEAN (see https://www.locean-ipsl.upmc.fr/smos/drifters/). Only validated data are considered with uncertainty order of 0.01 and 0.1.

1.2 Auxiliary geophysical datasets

Additional EO datasets are used to characterize the geophysical conditions at the *in situ* measurement locations and time, and 10 days prior to the measurements, to get an estimate of the geophysical concomitant condition and history. As discussed in Boutin et al. (2016), the presence of vertical gradients in, and horizontal variability of, sea surface salinity indeed complicates comparison of satellite and *in situ* measurements. The additional EO data are used here to get a first estimates of conditions for which L-band satellite SSS measured in the first centimeters of the upper ocean within a 50-150 km diameter footprint might differ from pointwise *in situ* measurements performed in general between 10 and 5 m depth below the surface. The spatio-temporal variability of SSS within a satellite footprint (50-150 km) is a major issue for satellite SSS validation in the vicinity of river plumes, frontal zones, and significant precipitation areas,

4

among others. Rainfall can in some cases produce vertical salinity gradients exceeding 1 pss m^{-1}; consequently, it is recommended that satellite and *in situ* SSS measurements less than 3–6 h after rain events should be considered with care when used in satellite calibration/validation analyses. To identify such situation, the Pi-MEP platform is first using CMORPH products to characterize the local value and history of rain rate and ASCAT gridded data are used to characterize the local surface wind speed and history. For validation purpose, the ISAS monthly SSS *in situ* analysed fields at 5 m depth are collocated and compared with the *in situ* SSS value. The use of ISAS is motivated by the fact that it is used in the SMOS L2 official validation protocol in which systematic comparisons of SMOS L2 retrieved SSS with ISAS are done. In complement to ISAS, annual std climatological field from the World Ocean Atlas (WOA13) at the *in situ* location are also used to have an a priori information of the local SSS variability.

1.2.1 CMORPH

Precipitation are estimated using the CMORPH 3-hourly products at 1/4° resolution (Joyce et al. (2004)). CMORPH (CPC MORPHing technique) produces global precipitation analyses at very high spatial and temporal resolution. This technique uses precipitation estimates that have been derived from low orbiter satellite microwave observations exclusively, and whose features are transported via spatial propagation information that is obtained entirely from geostationary satellite IR data. At present NOAA incorporate precipitation estimates derived from the passive microwaves aboard the DMSP 13, 14 and 15 (SSM/I), the NOAA-15, 16, 17 and 18 (AMSU-B), and AMSR-E and TMI aboard NASA's Aqua, TRMM and GPM spacecraft, respectively. These estimates are generated by algorithms of Ferraro (1997) for SSM/I, Ferraro et al. (2000) for AMSU-B and Kummerow et al. (2001) for TMI. Note that this technique is not a precipitation estimation algorithm but a means by which estimates from existing microwave rainfall algorithms can be combined. Therefore, this method is extremely flexible such that any precipitation estimates from any microwave satellite source can be incorporated.

With regard to spatial resolution, although the precipitation estimates are available on a grid with a spacing of 8 km (at the equator), the resolution of the individual satellite-derived estimates is coarser than that - more on the order of 12 x 15 km or so. The finer "resolution" is obtained via interpolation.

In effect, IR data are used as a means to transport the microwave-derived precipitation features during periods when microwave data are not available at a location. Propagation vector matrices are produced by computing spatial lag correlations on successive images of geostationary satellite IR which are then used to propagate the microwave derived precipitation estimates. This process governs the movement of the precipitation features only. At a given location, the shape and intensity of the precipitation features in the intervening half hour periods between microwave scans are determined by performing a time-weighting interpolation between microwave-derived features that have been propagated forward in time from the previous microwave observation and those that have been propagated backward in time from the following microwave scan. NOAA refer to this latter step as "morphing" of the features.

For the present Pi-MEP products, we only considered the 3-hourly products at 1/4 degree resolution. The entire CMORPH record (December 2002-present) for 3-hourly, 1/4 degree lat/lon resolution can be found at: `ftp://ftp.cpc.ncep.noaa.gov/precip/CMORPH_V1.0/CRT/`. CMORPH estimates cover a global belt (-180°W to 180°E) extending from 60°S to 60°N latitude and are available for the complete period of the Pi-MEP core datasets (Jan 2010-now).

1.2.2 ASCAT

Advanced SCATterometer (ASCAT) daily data produced and made available at Ifremer/CERSAT on a 0.25°x0.25° resolution grid (Bentamy and Fillon (2012)) since March 2007 are used to characterize the mean daily wind at the match-up pair location as well as the wind history during the 10-days period preceding the in situ measurement date. These wind fields are calculated based on a geostatistical method with external drift. Remotely sensed data from ASCAT are considered as observations while those from numerical model analysis (ECMWF) are associated with the external drift. The spatial and temporal structure functions for wind speed, zonal and meridional wind components are estimated from ASCAT retrievals. Furthermore, the new procedure includes a temporal interpolation of the retrievals based on the complex empirical orthogonal function (CEOF) approach, in order to enhance the sampling length of the scatterometer observations. The resulting daily wind fields involves the main known surface wind patterns as well as some variation modes associated with temporal and spatial moving features. The accuracy of the gridded winds was investigated through comparisons with moored buoy data in Bentamy et al. (2012) and resulted in rms differences for wind speed and direction are about 1.50 m.s^{-1} and 20°.

1.2.3 ISAS

The In Situ Analysis System (ISAS), as described in Gaillard et al. (2016) is a data based reanalysis of temperature and salinity fields over the global ocean 70°N–70°S on a 1/2° grid. It was initially designed to synthesize the temperature and salinity profiles collected by the Argo program. It has been later extended to accommodate all type of vertical profile as well as time series. ISAS gridded fields are entirely based on *in situ* measurements. The methodology and configuration have been conceived to preserve as much as possible the data information content and resolution. ISAS is developed and run in a research laboratory (LOPS) in close collaboration with Coriolis, one of Argo Global Data Assembly Center and unique data provider for the Mercator operational oceanography system. In Pi-MEP, the products used are the IN-SITU_GLO_TS_OA_REP_OBSERVATIONS_013_002_b for the period 2010 to 2019 and the IN-SITU_GLO_TS_OA_NRT_OBSERVATIONS_013_002_a for the Near-Real Time (2020-2021) derived at the Coriolis data center and provided by the Copernicus Marine Environment Monitoring Service (CMEMS). The major contribution to the data set is from Argo array of profiling floats, reaching an approximate resolution of one profile every 10-days and every 3-degrees over the satellite SSS period (http://www.umr-lops.fr/SNO-Argo/Products/ISAS-T-S-fields/); in this version SSS from ship of opportunity thermosalinographs are not used, so that we can consider SMOS SSS validation using these measurements independent of ISAS. The ISAS optimal interpolation involves a structure function modeled as the sum of two Gaussian functions, each associated with specific time and space scales, resulting in a smoothing over typically 3 degrees. The smallest scale which can be retrieved with ISAS analysis is not smaller than 300–500 km (Kolodziejczyk et al. (2015)). For validation purpose, the ISAS monthly SSS fields at 5 m depth are collocated and compared with the satellite SSS products and included in the Pi-MEP Match-up files. In addition, the "percentage of variance" fields (PCTVAR) contained in the ISAS analyses provide information on the local variability of *in situ* SSS measurements within 1/2°x1/2° boxes.

1.2.4 World Ocean Atlas Climatology

The World Ocean Atlas 2013 version 2 (WOA13 V2) is a set of objectively analyzed (1° grid) climatological fields of *in situ* temperature, salinity and other variables provided at standard

depth levels for annual, seasonal, and monthly compositing periods for the World Ocean. It also includes associated statistical fields of observed oceanographic profile data interpolated to standard depth levels on 5°, 1°, and 0.25° grids. We use these fields in complement to ISAS to characterize the climatological fields (annual mean and std) at the match-up pairs location and date.

2 In Situ Dababase Analyses

2.1 Introduction

The skin depth of the L-band radiometer signal over the ocean is about 1 cm whereas classical surface salinity measured by ships or Argo floats are performed at a few meters depth. In order to improve the knowledge of the SSS variability in the first 50 cm depth, to better document the SSS variability in a satellite pixel and to provide ground-truth as close as possible to the sea surface for validating satellite SSS, the L-band remotely sensed community proposed to deploy numerous surface drifters over various parts of the ocean. Surface drifter data are provided by the LOCEAN (see https://www.locean-ipsl.upmc.fr/smos/drifters/). Only validated data are considered with uncertainty order of 0.01 and 0.1.

2.2 Number of SSS data as a function of time and distance to coast

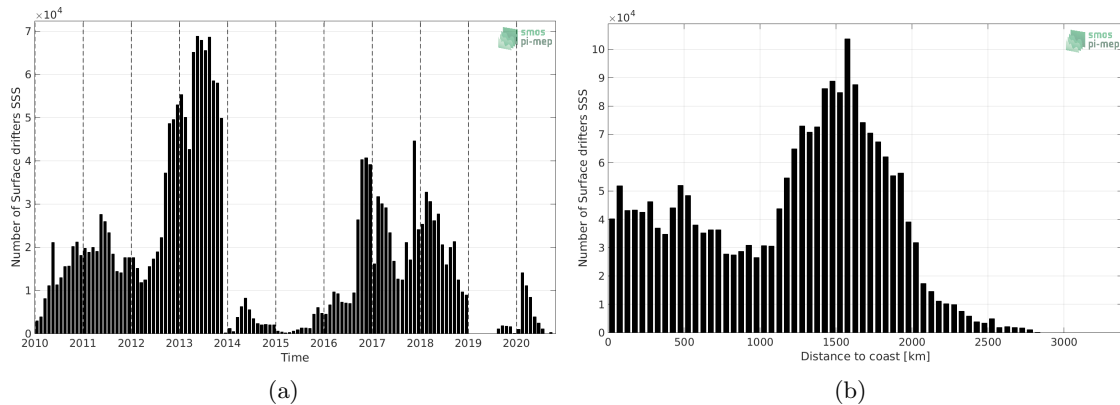Figure 1 shows the time (a) and distance to coast (b) distributions of the Surface drifters *in situ* dataset.

(a)	(b)

Figure 1: Number of SSS from Surface drifters as a function of time (a) and distance to coast (b).

2.3 Histograms of SSS

Figure 2 shows the SSS distribution of the Surface drifters (a) and colocalized ISAS (b) dataset.
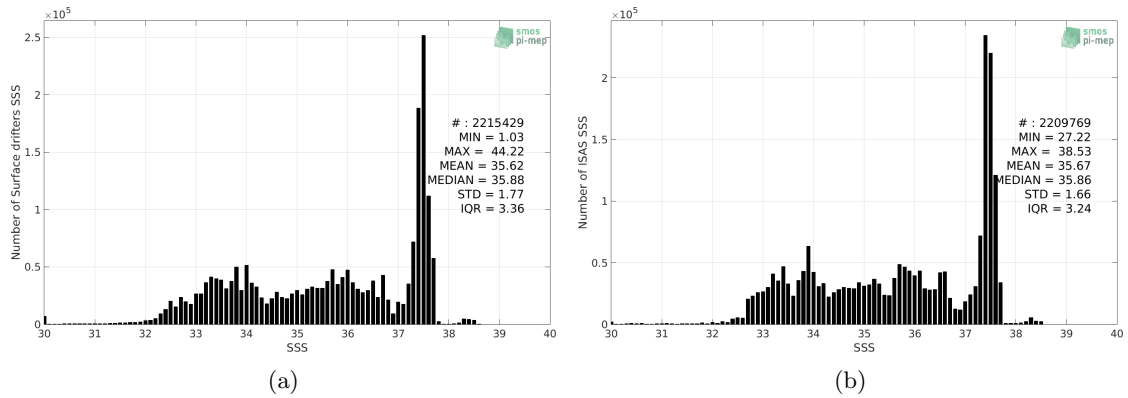
Figure 2: Histograms of SSS from Surface drifters (a) and ISAS (b) per bins of 0.1.

2.4 Distribution of *in situ* SSS depth measurements

In Figure 3, we show the depth distribution of the *in situ* salinity dataset (a) and the spatial distribution of the depth temporal mean in 1°x1° boxes and considering the full *in situ* dataset period (b).
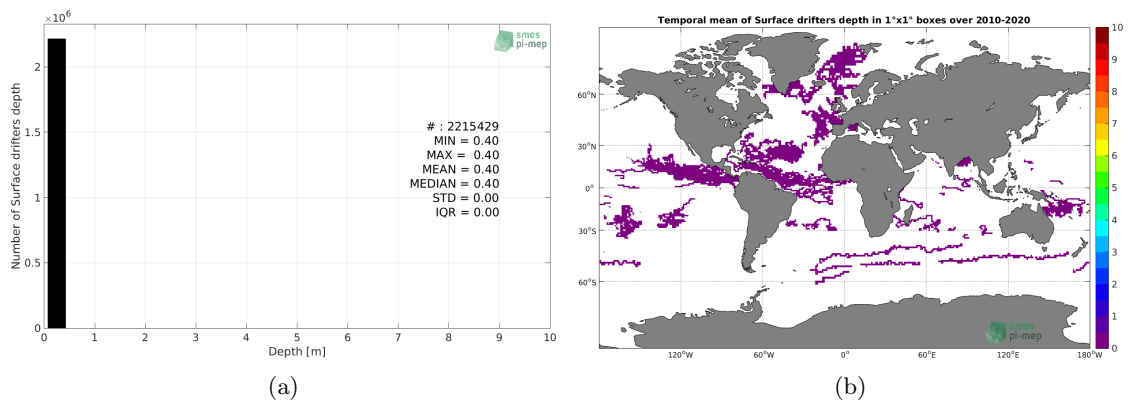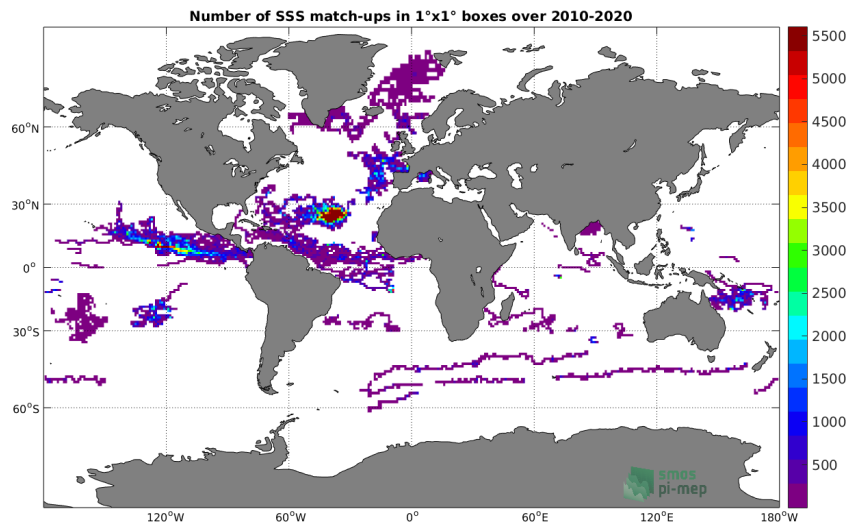

Figure 3: Depth distribution of the upper level SSS measurements from Surface drifters (a) and spatial distribution of the *in situ* SSS depth measurements showing the mean value in 1°x1° boxes and considering the full *in situ* dataset period (b).

2.5 Spatial distribution of SSS

In Figure 4, the number of Surface drifters SSS measurements in 1°x1° boxes is shown.

Figure 4: Number of SSS from Surface drifters in 1°x1° boxes.

2.6 Spatial Maps of the Temporal mean and Std of *in situ* and ISAS SSS and of the difference (ΔSSS)

In Figure 5, maps of temporal mean (left) and standard deviation (right) of ISAS (top), Surface drifters *in situ* dataset (middle) and the difference ΔSSS(ISAS -Surface drifters) (bottom) are shown. The temporal mean and std are calculated using all match-up pairs falling in spatial boxes of size 1°x1° over the full Surface drifters dataset period.
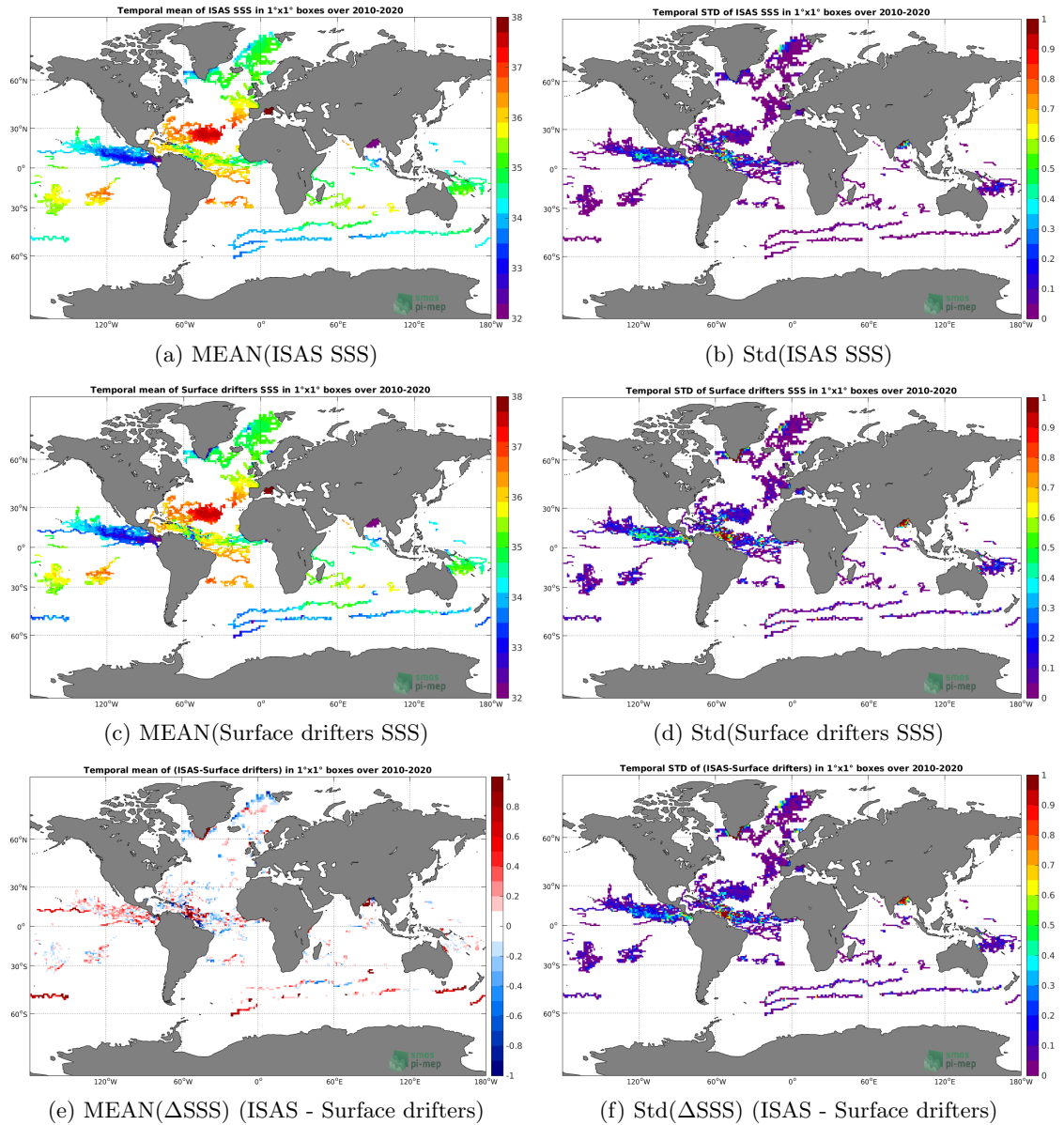
(a) MEAN(ISAS SSS)

(b) Std(ISAS SSS)

(c) MEAN(Surface drifters SSS)

(d) Std(Surface drifters SSS)

(e) MEAN(ΔSSS) (ISAS - Surface drifters)

(f) Std(ΔSSS) (ISAS - Surface drifters)

Figure 5: Temporal mean (left) and Std (right) of SSS from ISAS (top), Surface drifters (middle), and of ΔSSS (ISAS - Surface drifters). Only match-up pairs are used to generate these maps.

2.7 Time series of the monthly median and Std of *in situ* and ISAS SSS and of the difference (ΔSSS)

In the top panel of Figure 6, we show the time series of the monthly median SSS estimated for both ISAS SSS product (in black) and the Surface drifters *in situ* dataset (in blue) at the collected Pi-MEP match-up pairs.

In the middle panel of Figure 6, we show the time series of the monthly median of ΔSSS (ISAS - Surface drifters) for the collected Pi-MEP match-up pairs.

In the bottom panel of Figure 6, we show the time series of the monthly standard deviation of the ΔSSS (ISAS - Surface drifters) for the collected Pi-MEP match-up pairs.
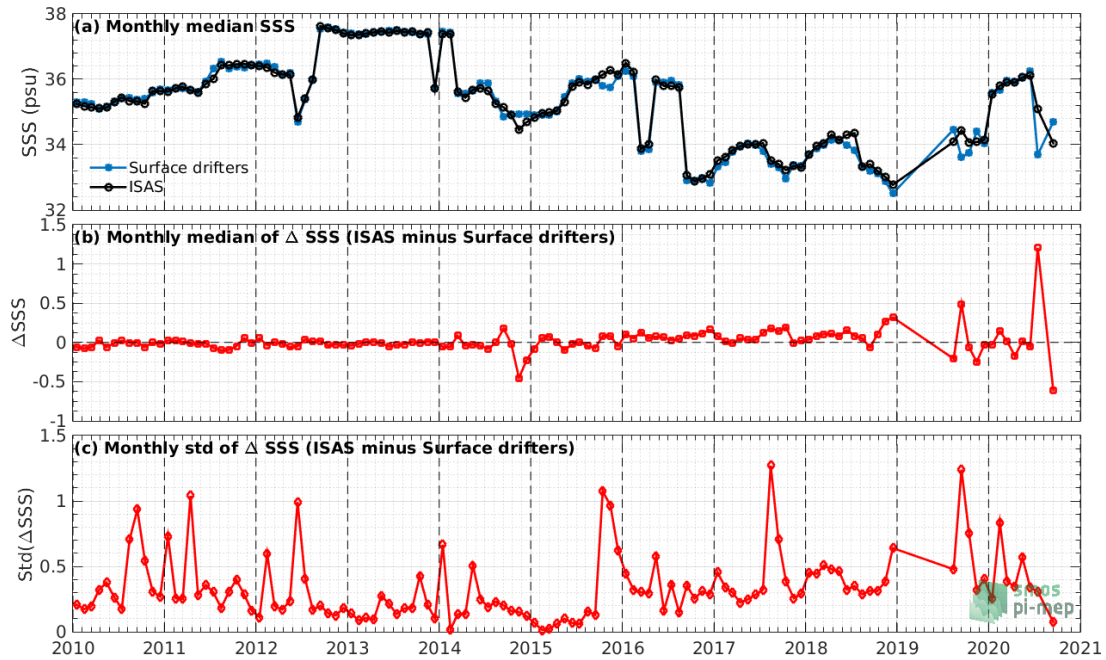

Figure 6: Time series of the monthly median SSS (top), median of ΔSSS (ISAS - Surface drifters) and Std of ΔSSS (ISAS - Surface drifters) considering all match-ups collected by the Pi-MEP.

2.8 Zonal mean and Std of *in situ* and ISAS SSS and of the difference ΔSSS

In Figure 7 left panel, we show the zonal mean SSS considering all Pi-MEP match-up pairs for both ISAS SSS product (in black) and the Surface drifters *in situ* dataset (in blue). The full *in situ* dataset period is used to derive the mean.

In the right panel of Figure 7, we show the zonal mean of ΔSSS (ISAS - Surface drifters) for all the collected Pi-MEP match-up pairs estimated over the full *in situ* dataset period.
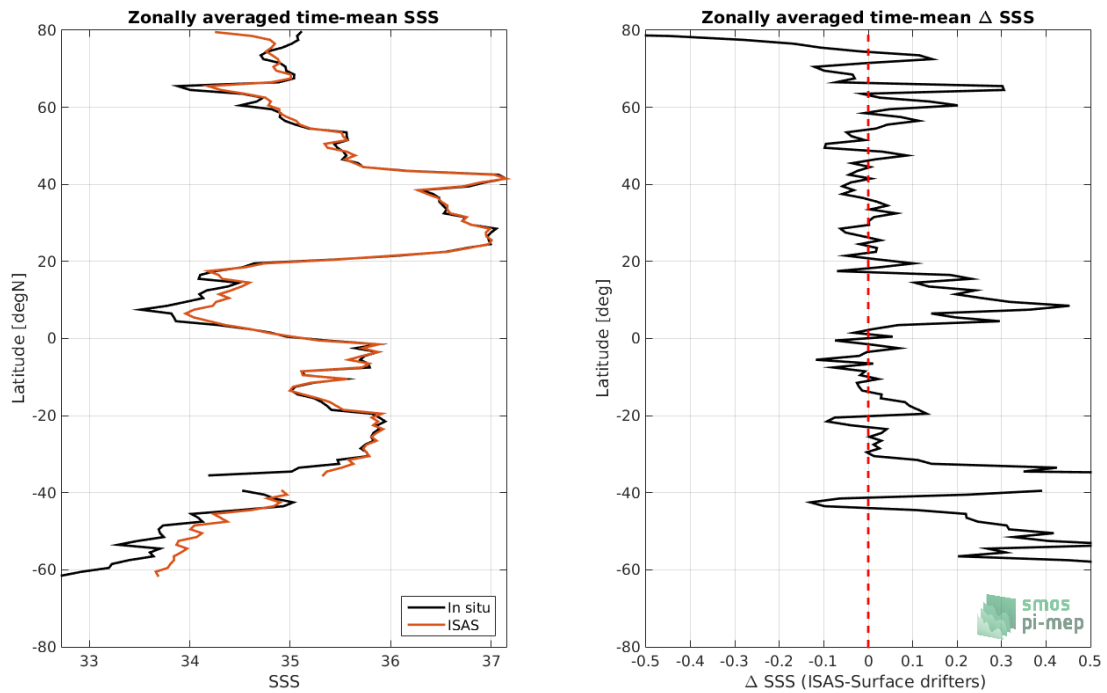
Figure 7: Left panel: Zonal mean SSS from ISAS product (black) and from Surface drifters (blue). Right panel: Zonal mean of ΔSSS (ISAS - Surface drifters) for all the collected Pi-MEP match-up pairs estimated over the full *in situ* dataset period.

2.9 Scatterplots of ISAS vs *in situ* SSS by latitudinal bands

In Figure 8, contour maps of the concentration of ISAS SSS (y-axis) versus Surface drifters SSS (x-axis) at match-up pairs for different latitude bands: (a) 80°S-80°N, (b) 20°S-20°N, (c) 40°S-20°S and 20°N-40°N and (d) 60°S-40°S and 40°N-60°N. For each plot, the red line shows x=y. The black thin and dashed lines indicate a linear fit through the data cloud and the $\pm 95\%$ confidence levels, respectively. The number match-up pairs n, the slope and R^2 coefficient of the linear fit, the root mean square (RMS) and the mean bias between ISAS and *in situ* data are indicated for each latitude band in each plots.

(a) $0° \leq |\mathrm{LAT}| \leq 80°$

(b) $0° \leq |\mathrm{LAT}| \leq 20°$

(c) $20° \leq |\mathrm{LAT}| \leq 40°$
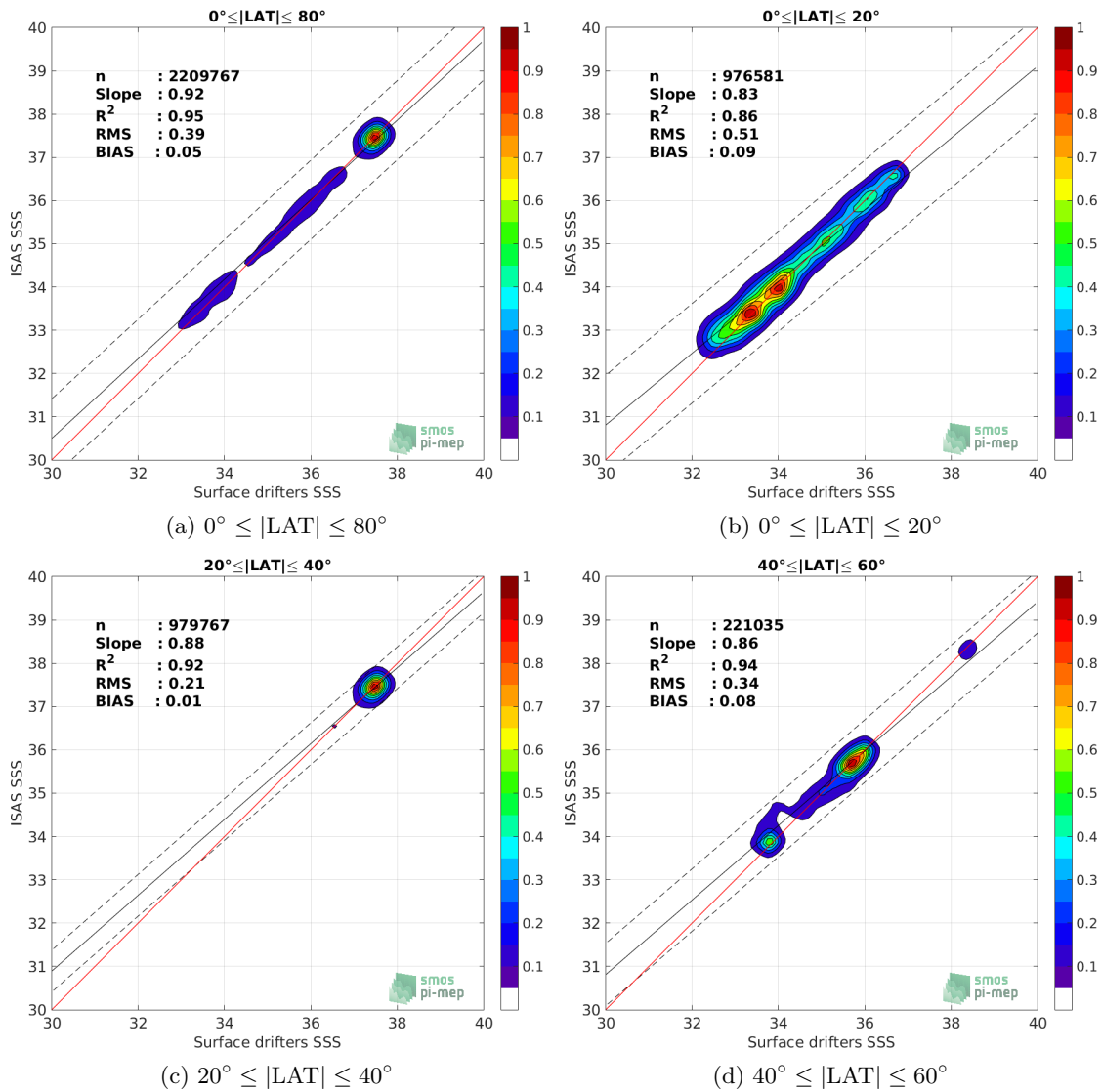
(d) $40° \leq |\mathrm{LAT}| \leq 60°$

Figure 8: Contour maps of the concentration of ISAS SSS (y-axis) versus Surface drifters SSS (x-axis) at match-up pairs for different latitude bands. For each plot, the red line shows x=y. The black thin and dashed lines indicate a linear fit through the data cloud and the ±95% confidence levels, respectively. The number match-up pairs n, the slope and R^2 coefficient of the linear fit, the root mean square (RMS) and the mean bias between ISAS and *in situ* data are indicated for each latitude band in each plots.

2.10   Time series of the monthly median and Std of the difference ΔSSS sorted by latitudinal bands

In Figure 9, time series of the monthly median (red curves) of ΔSSS (ISAS - Surface drifters) and ±1 Std (black vertical thick bars) as function of time for all the collected Pi-MEP match-up pairs estimated for the full *in situ* dataset period are shown for different latitude bands: (a) 80°S-80°N, (b) 20°S-20°N, (c) 40°S-20°S and 20°N-40°N and (d) 60°S-40°S and 40°N-60°N.

13

Figure 9: Monthly median (red curves) of ΔSSS (ISAS - Surface drifters) and ±1 Std (black vertical thick bars) as function of time for all the collected Pi-MEP match-up pairs for the full *in situ* dataset period are shown for different latitude bands: (a) 80°S-80°N, (b) 20°S-20°N, (c) 40°S-20°S and 20°N-40°N and (d) 60°S-40°S and 40°N-60°N.
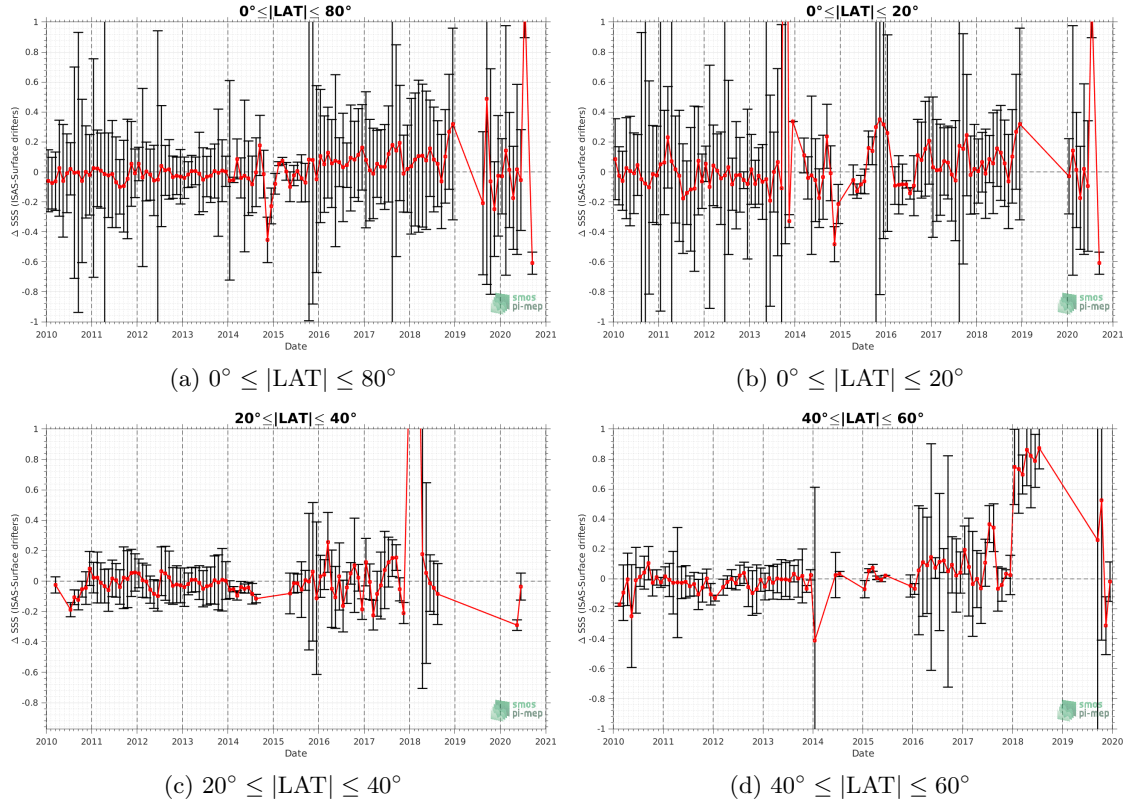
2.11 ΔSSS sorted as geophysical conditions

In Figure 10, we classify the match-up differences ΔSSS (ISAS - *in situ*) as function of the geophysical conditions at match-up points. The mean and std of ΔSSS (ISAS - Surface drifters) is thus evaluated as function of the

- *in situ* SSS values per bins of width 0.2,
- *in situ* SST values per bins of width 1°C,
- ASCAT daily wind values per bins of width 1 m/s,
- CMORPH 3-hourly rain rates per bins of width 1 mm/h, and,
- distance to coasts per bins of width 50 km,
- *in situ* measurement depth (if relevant).

(a) Surface drifters SSS

(b) Surface drifters SST

(c) ASCAT Wind Speed

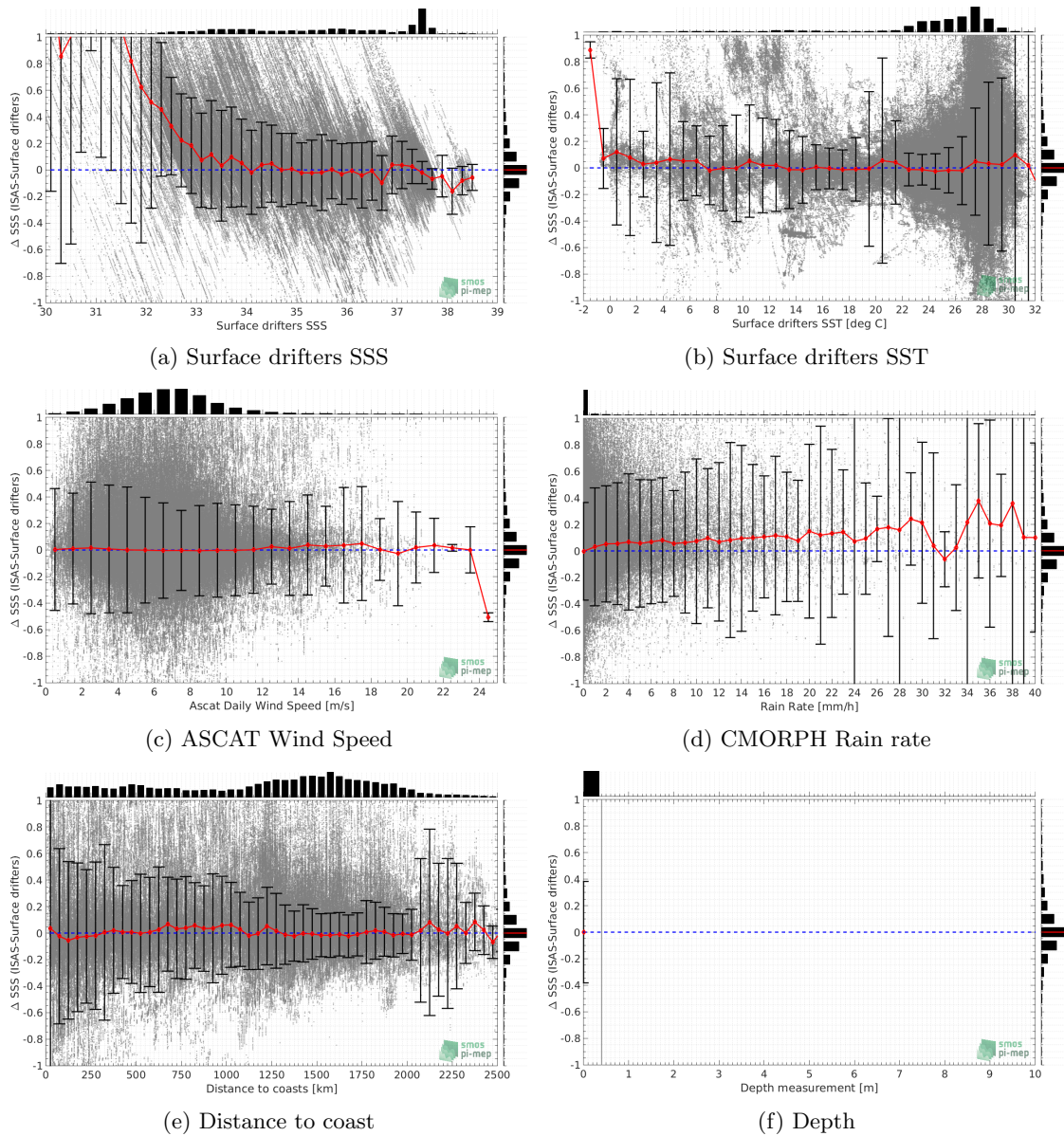(d) CMORPH Rain rate

(e) Distance to coast

(f) Depth

Figure 10: Δ SSS (ISAS - Surface drifters) sorted as geophysical conditions: Surface drifters SSS a), Surface drifters SST b), ASCAT Wind speed c), CMORPH rain rate d), distance to coast (e) and depth measurements (f).

2.12 ΔSSS maps and statistics for different geophysical conditions

In Figures 11 and 12, we focus on sub-datasets of the match-up differences ΔSSS (ISAS - *in situ*) for the following specific geophysical conditions:

- **C1**:if the local value at *in situ* location of estimated rain rate is zero, mean daily wind is in the range [3, 12] m/s, the SST is > 5°C and distance to coast is > 800 km.

15

- **C2**:if the local value at *in situ* location of estimated rain rate is zero, mean daily wind is in the range [3, 12] m/s.

- **C3**:if the local value at *in situ* location of estimated rain rate is high (ie. > 1 mm/h) and mean daily wind is low (ie. < 4 m/s).

- **C5**:if the *in situ* data is located where the climatological SSS standard deviation is low (ie. above < 0.2).

- **C6**:if the *in situ* data is located where the climatological SSS standard deviation is high (ie. above > 0.2).

For each of these conditions, the temporal mean (gridded over spatial boxes of size 1°x1°) and the histogram of the difference ΔSSS (ISAS - *in situ*) are presented.

(a) RR=0 mm/h, 3< U_{10} <12 m/s, SST>5°C, distance to coast > 800 km
(b) RR=0 mm/h, 3< U_{10} <12 m/s
(c) RR>1mm/h and U_{10} <4m/s
(d) WOA2013 SSS Std<0.2
(e) WOA2013 SSS Std>0.2
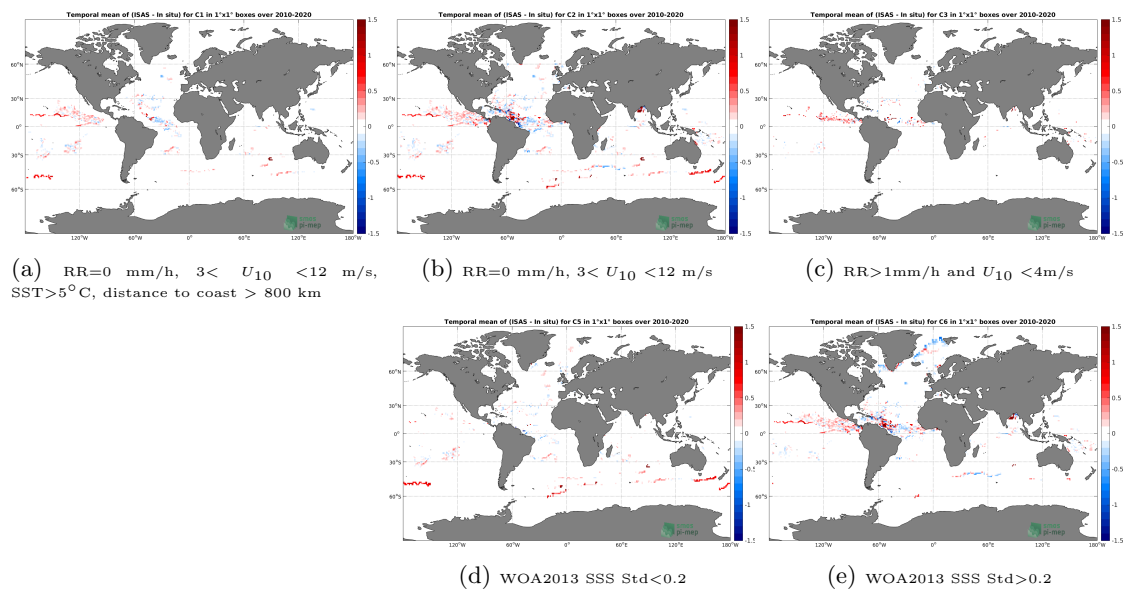
Figure 11: Temporal mean gridded over spatial boxes of size 1°x1° of ΔSSS (ISAS - Surface drifters) for 5 different subdatasets corresponding to:RR=0 mm/h, 3< U_{10} <12 m/s, SST>5°C, distance to coast > 800 km (a), RR=0 mm/h, 3< U_{10} <12 m/s (b), RR>1mm/h and U_{10} <4m/s (c),WOA2013 SSS Std<0.2 (d),WOA2013 SSS Std>0.2 (e).

(a) RR=0 mm/h, 3< U_{10} <12 m/s, SST>5°C, distance to coast > 800 km

(b) RR=0 mm/h, 3< U_{10} <12 m/s

(c) RR>1mm/h and U_{10} <4m/s

(d) WOA2013 SSS Std<0.2
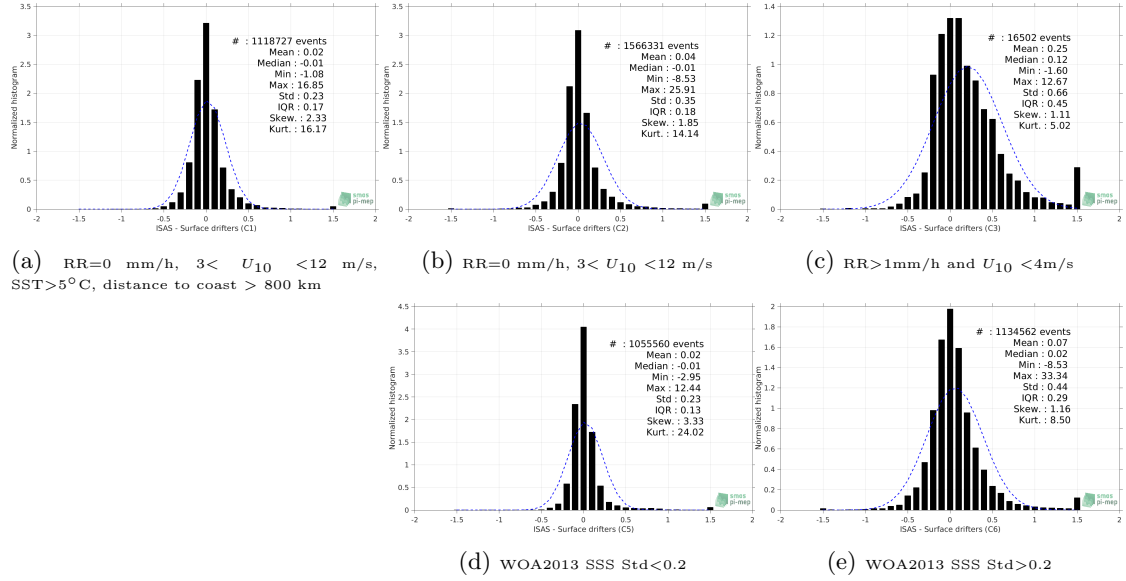
(e) WOA2013 SSS Std>0.2

Figure 12: Normalized histogram of ΔSSS (ISAS - Surface drifters) for 5 different subdatasets corresponding to:RR=0 mm/h, 3< U_{10} <12 m/s, SST>5°C, distance to coast > 800 km (a), RR=0 mm/h, 3< U_{10} <12 m/s (b), RR>1mm/h and U_{10} <4m/s (c),WOA2013 SSS Std<0.2 (d),WOA2013 SSS Std>0.2 (e).

2.13   Summary

Table 1 shows the mean, median, standard deviation (Std), root mean square (RMS), interquartile range (IQR), correlation coefficient (r^2) and robust standard deviation (Std*) of the match-up differences ΔSSS (ISAS - Surface drifters) for the following conditions:

- all: All the match-up pairs satellite/in situ SSS values are used to derive the statistics

- C1: only pairs where RR=0 mm/h, 3< U_{10} <12 m/s, SST>5°C, distance to coast > 800 km

- C2: only pairs where RR=0 mm/h, 3< U_{10} <12 m/s

- C3: only pairs where RR>1mm/h and U_{10} <4m/s

- C5: only pairs where WOA2013 SSS Std<0.2

- C6: only pairs where WOA2013 SSS Std>0.2

- C7a: only pairs with a distance to coast < 150 km.

- C7b: only pairs with a distance to coast in the range [150, 800] km.

- C7c: only pairs with a distance to coast > 800 km.

- C8a: only pairs where SST is < 5°C.

- C8b: only pairs where SST is in the range [5, 15]°C.

- C8c: only pairs where SST is > 15°C.

17

- C9a: only pairs where SSS is < 33.

- C9b: only pairs where SSS is in the range $[33, 37]$.

- C9c: only pairs where SSS is > 37.

Table 1: Statistics of ΔSSS (ISAS - Surface drifters)

Condition	#	Median	Mean	Std	RMS	IQR	r^2	Std*
all	2209769	0.00	0.05	0.38	0.39	0.19	0.954	0.14
C1	1118727	-0.01	0.02	0.23	0.23	0.17	0.982	0.13
C2	1566331	-0.01	0.04	0.35	0.35	0.18	0.957	0.13
C3	16502	0.12	0.25	0.66	0.71	0.45	0.844	0.32
C5	1055560	-0.01	0.02	0.23	0.23	0.13	0.965	0.10
C6	1134562	0.02	0.07	0.44	0.45	0.29	0.928	0.21
C7a	131297	-0.02	0.13	0.91	0.91	0.30	0.798	0.21
C7b	519947	0.01	0.08	0.47	0.47	0.21	0.871	0.16
C7c	1558469	0.00	0.04	0.25	0.26	0.19	0.981	0.14
C8a	33057	0.07	0.23	0.55	0.60	0.13	0.467	0.09
C8b	144866	0.01	0.08	0.33	0.34	0.16	0.923	0.12
C8c	2026237	0.00	0.05	0.38	0.38	0.20	0.955	0.14
C9a	165932	0.29	0.50	0.97	1.10	0.44	0.153	0.32
C9b	1283786	0.01	0.03	0.31	0.31	0.24	0.929	0.18
C9c	760051	-0.02	-0.02	0.11	0.11	0.11	0.707	0.08

Table 1 numerical values can be downloaded as a csv file here.

References

Abderrahim Bentamy and Denis Croize Fillon. Gridded surface wind fields from Metop/ASCAT measurements. *Int. J. Remote Sens.*, 33(6):1729–1754, March 2012. ISSN 1366-5901. doi: 10.1080/01431161.2011.600348.

Abderrahim Bentamy, Semyon A. Grodsky, James A. Carton, Denis Croizé-Fillon, and Bertrand Chapron. Matching ASCAT and QuikSCAT winds. *J. Geophys. Res.*, 117(C2), February 2012. ISSN 0148-0227. doi: 10.1029/2011JC007479.

Jaqueline Boutin, Y. Chao, W. E. Asher, T. Delcroix, R. Drucker, K. Drushka, N. Kolodziejczyk, T. Lee, N. Reul, G. Reverdin, J. Schanze, A. Soloviev, L. Yu, J. Anderson, L. Brucker, E. Dinnat, A. S. Garcia, W. L. Jones, C. Maes, T. Meissner, W. Tang, N. Vinogradova, and B. Ward. Satellite and In Situ Salinity: Understanding Near-Surface Stratification and Sub-footprint Variability. *Bull. Am. Meterol. Soc.*, 97(8):1391–1407, 2016. ISSN 1520-0477. doi: 10.1175/bams-d-15-00032.1.

Ralph R. Ferraro. SSM/I derived global rainfall estimates for climatological applications. *J. Geophys. Res.*, 102(D14):16715–16736, 07 1997. doi: 10.1029/97JD01210.

Ralph R. Ferraro, Fuzhong Weng, Norman C. Grody, and Limin Zhao. Precipitation characteristics over land from the NOAA-15 AMSU sensor. *Geophys. Res. Lett.*, 27(17):2669–2672, 2000. doi: 10.1029/2000GL011665.

Fabienne Gaillard, Thierry Reynaud, Virginie Thierry, Nicolas Kolodziejczyk, and Karina von Schuckmann. In Situ-Based Reanalysis of the Global Ocean Temperature and Salinity with ISAS: Variability of the Heat Content and Steric Height. *J. Clim.*, 29(4):1305–1323, February 2016. ISSN 1520-0442. doi: 10.1175/jcli-d-15-0028.1.

Robert J. Joyce, John E. Janowiak, Phillip A. Arkin, and Pingping Xie. CMORPH: A Method that Produces Global Precipitation Estimates from Passive Microwave and Infrared Data at High Spatial and Temporal Resolution. *J. Hydrometeorol.*, 5(3):487–503, June 2004. doi: 10.1175/1525-7541(2004)005⟨0487:camtpg⟩2.0.co;2.

Nicolas Kolodziejczyk, Gilles Reverdin, and Alban Lazar. Interannual Variability of the Mixed Layer Winter Convection and Spice Injection in the Eastern Subtropical North Atlantic. *J. Phys. Oceanogr.*, 45(2):504–525, Feb 2015. ISSN 1520-0485. doi: 10.1175/jpo-d-14-0042.1.

Christian Kummerow, Y. Hong, W. S. Olson, S. Yang, R. F. Adler, J. McCollum, R. Ferraro, G. Petty, D-B. Shin, and T. T. Wilheit. The Evolution of the Goddard Profiling Algorithm (GPROF) for Rainfall Estimation from Passive Microwave Sensors. *J. Appl. Meteorol.*, 40(11): 1801–1820, 2001. doi: 10.1175/1520-0450(2001)040⟨1801:TEOTGP⟩2.0.CO;2.